NANO LETTERS

Letter

pubs.acs.org/NanoLett

# Solution Synthesis of Iodine-Doped Red Phosphorus Nanoparticles for Lithium-Ion Battery Anodes

Wei-Chung Chang, Kuan-Wei Tseng, and Hsing-Yu Tuan*

Department of Chemical Engineering, National Tsing Hua University, 101, Section 2, Kuang-Fu Road, Hsinchu, Taiwan 30013, ROC

Supporting Information

**ABSTRACT:** Red phosphorus (RP) is a promising anode material for lithium-ion batteries due to its earth abundance and a high theoretical capacity of 2596 mA h $g^{-1}$. Although RP-based anodes for lithium-ion batteries have been reported, they were all in the form of carbon−P composites, including P−graphene, P−graphite, P−carbon nanotubes (CNTs), and P−carbon black, to improve P's extremely low conductivity and large volume change during cycling process. Here, we report the large-scale synthesis of red phosphorus nanoparticles (RPNPs) with sizes ranging from 100 to 200 nm by reacting $PI_3$ with ethylene glycol in the presence of cetyltrimethylammonium bromide (CTAB) in ambient environment. Unlike the insulator behavior of commercial RP (conductivity of $<10^{-12}$ S $m^{-1}$), the conductivity of RPNPs is between $2.62 \times 10^{-3}$ and $1.81 \times 10^{-2}$ S $m^{-1}$, which is close to that of semiconductor germanium ($1.02 \times 10^{-2}$ S $m^{-1}$), and 2 orders of magnitude higher than silicon ($5.35 \times 10^{-4}$ S $m^{-1}$). Around 3−5 wt % of iodine-doping was found in RPNPs, which was speculated as the key to significantly improve the conductivity of RPNPs. The significantly improved conductivity of RPNPs and their uniform colloidal nanostructures enable them to be used solely as active materials for LIBs anodes. The RPNPs electrodes exhibit a high specific capacity of 1700 mA h $g^{-1}$ (0.2 C after 100 cycles, 1 C = 2000 mA $g^{-1}$), long cycling life (~900 mA h $g^{-1}$ after 500 cycles at 1 C), and outstanding rate capability (175 mA h $g^{-1}$ at the charge current density of 120 A $g^{-1}$, 60 C). Moreover, as a proof-of-concept example, pouch-type full cells using RPNPs anodes and $Li(Ni_{0.5}Co_{0.3}Mn_{0.2})O_2$ (NCM-532) cathodes were assembled to show their practical uses.

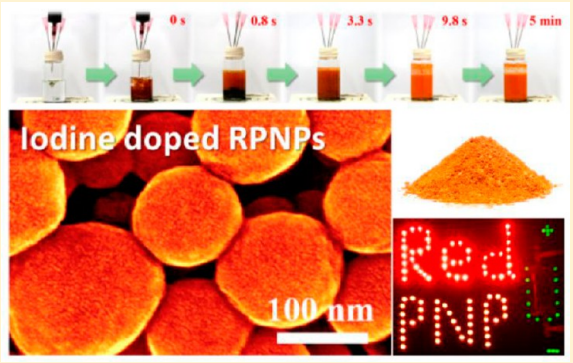


**KEYWORDS:** *Phosphorus, nanoparticles, iodine, solution-phase, lithium-ion batteries, anodes*

In the past 25 years, the energy density of lithium-ion batteries (LIBs) increased around 400%, which is mainly driven by the growing demanding from portable electronic devices and electric vehicles; however, it encounters the bottleneck due to mature development of anode−cathode configuration.[1] One effective way to increase the energy density of lithium ion battery is to replace the anode, i.e., graphite (372 mA h $g^{-1}$), by materials with a specific capacity above 1000 mA h $g^{-1}$, such as elemental silicon (Si) (3596 mA h $g^{-1}$), phosphorus (P) (2596 mA h $g^{-1}$), and germanium (Ge) (1384 mA h $g^{-1}$). Although, these high-capacity materials are known to be suffered from huge volume change during the lithiation−delithiation processes that result in pulverization, promising battery performance improvement was achieved through designs of nanostructures for Si and Ge[2−5] such as nanowires,[6−8] yolk−shell nanoparticles,[9,10] 3D porous nanoarchitecture,[11,12] and graphene-supported nanoparticles.[13] However, few studies focused on designing the nanostructure of P.

Phosphorus has three different allotropes: white phosphorus (WP), red phosphorus (RP), and black phosphorus (BP).[14] Among these three different allotropes, RP is the most promising anode material for LIBs because of its chemically stable property, nontoxic quality, low cost, and ease of fabrication. However, in addition to drastic volume expansion (300%)[15] during the process of lithiation−delithiation, RP has extremely low conductivity ($10^{-12}$ S $m^{-1}$)[16] to impede electron transport. To increase the P-based electrode conductivity, P have been modified by forming different type of carbon composites, such as P−graphite,[15,17,18] P−carbon black,[19−23] P−porous carbon,[24,25] P−CNT,[26,27] P−graphene,[28−31] and P-filled 3D carbon.[32] Nevertheless, there are several problems for P−C composites: (i) Obtaining stable cycling performance needs a high proportion of the low capacity carbon from 30 to 70%, results in the decrease of real battery energy density. (ii) The distribution of RP in the pores of carbon via the vaporization−condensation process is uncontrollable, and the loading ratio of P in the P−C composites is limited.[33] (iii) Traditional mechanical techniques such as ball-milling and hand-grinding result in broad sizes of particles.[34]

Herein, we demonstrated a solution-phase approach to synthesizing red phosphorus nanoparticles (RPNPs) in large scale in an ambient environment. In a typical reaction, $PI_3$ was

**Received:** December 7, 2016
**Revised:** January 9, 2017
**Published:** January 12, 2017





DOI: 10.1021/acs.nanolett.6b05081
*Nano Lett.* 2017, 17, 1240−1247

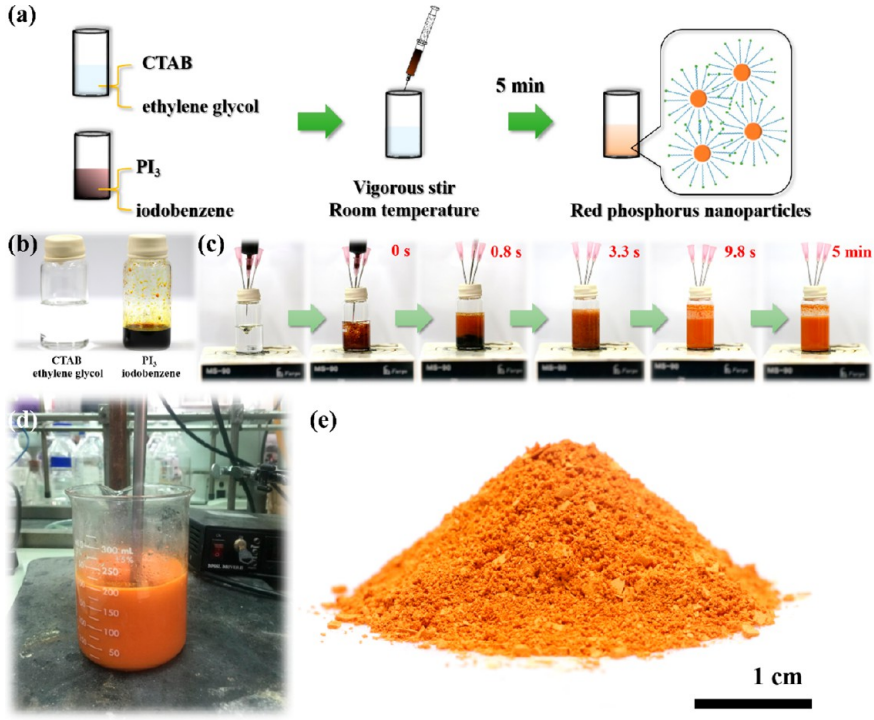


**Figure 1.** Synthesis of RPNPs. (a) Schematic design of RPNPs synthesis. (b) Image of CTAB solution and $PI_3$ solution. (c) The reaction process of RPNPs via the solution-phase approach. (d) Synthesis of RPNPs in large-scale (e) RPNPs powders (0.55 g).

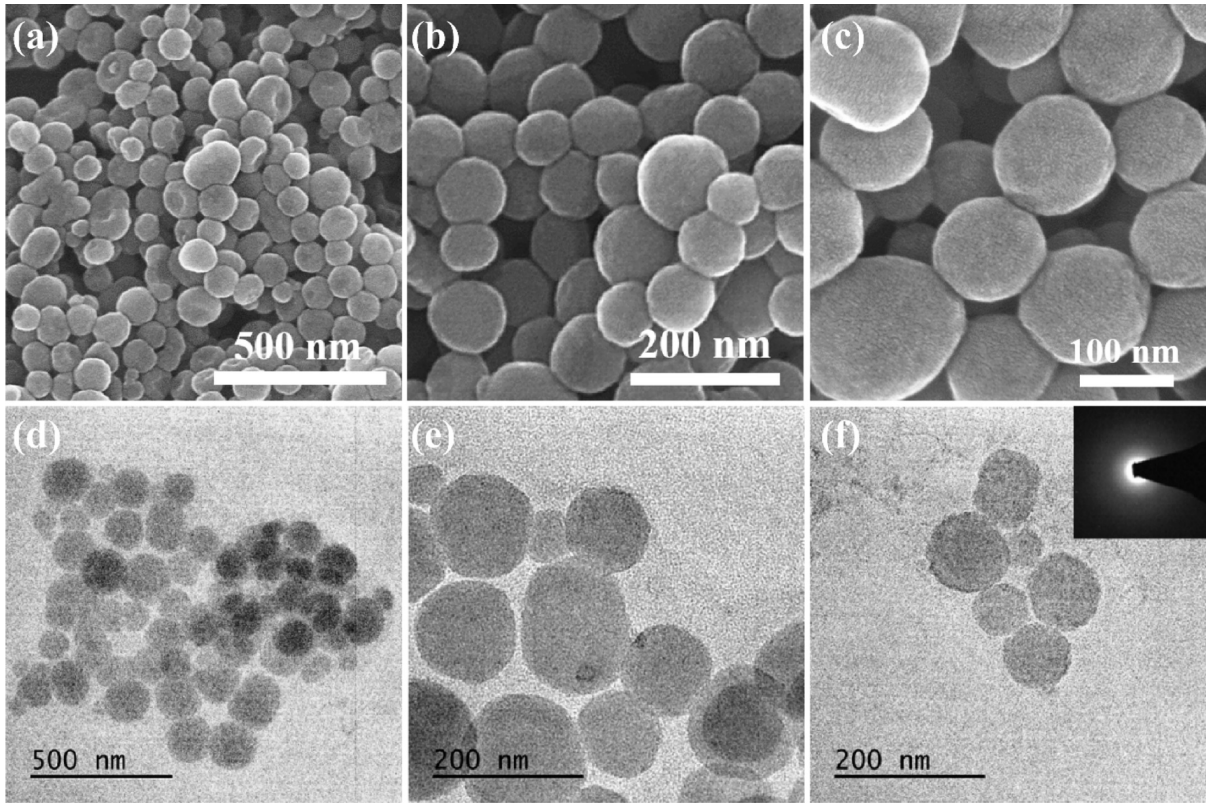


**Figure 2.** Morphology of RPNPs. (a–c) SEM images of RPNPs. (d–f) TEM images of RPNPs. The inset image is the SAED pattern.

reduced by ethylene glycol to generate RPNPs in the presence of CTAB. The electric measurement of pellets shows that conductivity of RPNPs is $10^{10}$ times higher than that of commercial RP, 100 times higher than that of Si, and slightly lower than that of Ge. Around 3–5 wt % iodine was found in RPNPs from analysis of EDS and XPS, which was speculated the key to significantly improve the conductivity of RPNPs. Therefore, RPNPs can be solely used as anode materials for LIBs without forming P–C composites and show very good battery performance. The improvement of conductivity and



DOI: 10.1021/acs.nanolett.6b05081
*Nano Lett.* 2017, 17, 1240–1247

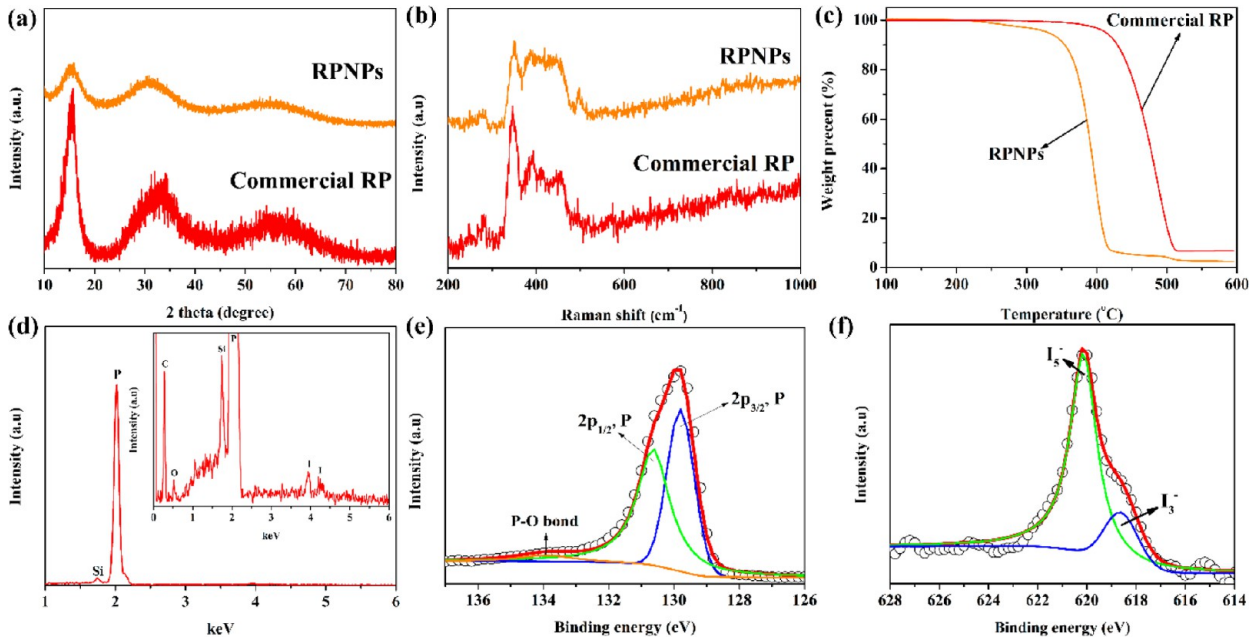


**Figure 3.** Characterization of RPNPs. (a) XRD patterns of RPNPs and commercial RP. (b) Raman spectra of RPNPs and commercial RP. (c) TGA of RPNPs and commercial RP. (d) EDS spectra of RPNPs. The inset image is the magnification. (e) $P2_p$ spectrum of XPS of RPNPs. (f) $I3_d5$ spectrum of XPS of RPNPs.

uniform nanosized morphology gives RPNPs good cycle stability (900 mA h $g^{-1}$ after 500 cycles at 1 C) and excellent ultrahigh rate capability (175 mA h $g^{-1}$ at the charge current density of 120 A $g^{-1}$, 60 C) in lithium-ion batteries. Finally, the performance of the full cell assembled by using RPNPs as anode and commercial $Li(Ni_{0.5}Co_{0.3}Mn_{0.2})O_2$ (NCM-532) as the cathode was evaluated, demonstrating the feasibility of RPNPs as an LIB anode.

**Results and Discussion.** Red phosphorus nanoparticles (RPNPs) with uniform size and near-spherical morphology could be facilely synthesized at room temperature using a solution-phase approach, as shown schematically in Figure 1a. The reaction of the solution-phase approach involved the reduction of $PI_3$ with ethylene glycol in the presence of CTAB. Briefly, in this process, $PI_3$ was used as a source of phosphorus, and ethylene glycol served as a reducing agent, while CTAB acted as a surfactant to limit the growth of phosphorus to form the phosphorus nanoparticles. Without the use of CTAB, the growth of phosphorus is uncontrollable, resulting in the formation of bulky red phosphorus crystals, as shown in Figure S1. In a typical process, a solution of CTAB in ethylene glycol and a solution of $PI_3$ in iodobenzene were prepared in advance (Figure 1b). The solution of $PI_3$ was then injected into the solution of CTAB under vigorously stirring (1050 rpm). The solution color changed rapidly to orange in 10 s, indicating the formation of RPNPs (Figure 1c). The yield of RPNPs, based on the amount of P atoms in $PI_3$, was approximately 20%. Furthermore, this solution-phase approach could be easily scale up to obtain large amounts of RPNPs. As shown in Figure 1d,e, the reaction carried out in a batch reactor could yield 0.2 g of RPNPs, providing sufficient active materials to prepare electrode. The color of the RPNPs was light orange, differing from the deep red color of commercial RP (Figure S2).

Figure 2 shows the majority of RPNPs synthesized appear with near-spherical shape with sizes ranging from 100 to 200 nm in diameter. The corresponding SAED pattern of RPNPs is shown in the inset image of Figure 2f, which revealed that RPNPs were amorphous structure. In other to further understand the structure of RPNPs, XRD patterns and Raman spectra were studied as shown in panels a and b of Figure 3, respectively. Its XRD pattern was dominated by three broadened diffraction peaks at 13−16°, 25−38°, and 47−65°, consistent with the XRD pattern of commercial RP reported in the literature.[20,30] Likewise, the Raman spectrum obtained for RPNPs was similar to the spectrum of commercial RP with the presence of three bands between 300 and 500 $cm^{-1}$. The thermal gravimetric analysis (TGA) of RPNPs in Figure 3c shows a sharp weight loss between 350 and 400 °C under a nitrogen atmosphere, whereas commercial RP shows a sharp weight loss between 450 and 500 °C. The observed phenomenon of sublimation temperature depression in TGA may result from high surface-to-volume ratios of nanoparticles.[35] To further corroborate the elemental compositions of RPNPs, energy-dispersive X-ray spectroscopy (EDS) and X-ray photoelectron spectroscopy (XPS) measurements were carried out (Figure 3d,e). The EDS spectra shows that RPNPs is almost completely composed of elemental phosphorus. $P2_p$ spectrum of XPS is fitted and separated into two peaks at 129.75 and 130.65 eV, which correspond to the P−P bond, according to the previous literature.[15,18] Moreover, a small fitting peak was found at 133.89 eV, which can be assigned to the P−O bond.[18,30] The surfaces of RPNPs are possibly oxidative when exposed to the air. Interestingly, among the analysis, we observed that slight iodine (3−5%) was doped into RPNPs from EDS spectra, as shown in the inset image of Figure 3d (Table S1 shows the EDS elemental compositions of RPNPs). XPS on $I3_d5$ spectrum in Figure 3f provides further evidence of iodine doping. $I3_d5$ spectrum is fitted to two peaks at around 618.5 and 620.1 eV, assigned to $I_3^-$ and $I_5^-$, respectively.[36,37]

To further investigate the property of RPNPs, the current−voltage ($I$−$V$) characteristic of a pellet tailored to the area of 0.25 $cm^2$ have been measured by a simple device, as shown in Figure 4a (Figure S3 shows the pellets before tailoring). The


DOI: 10.1021/acs.nanolett.6b05081
Nano Lett. 2017, 17, 1240−1247

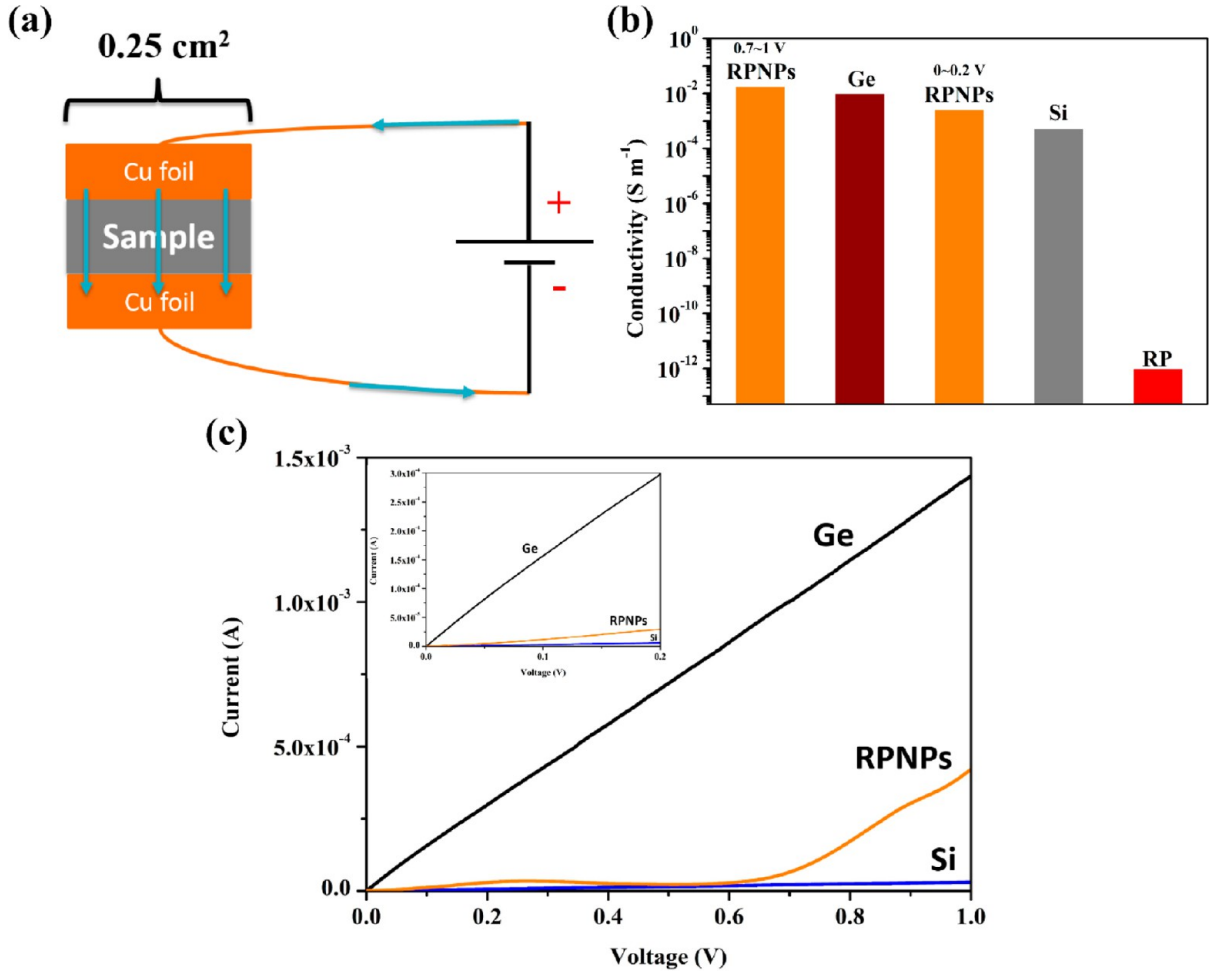


**Figure 4.** Electric characteristic of RPNPs, Ge, Si, and RP. (a) Schematic design of measuring device. (b) Comparison of conductivity of Ge, Si, RPNPs, and RP. (c) *I*−*V* curves of Ge, RPNPs, and Si. The inset image is the *I*−*V* curve, ranging from 0−0.2 V.

reliability of the device have been confirmed by measuring the conductivity of the Si and Ge pellets, showing that the results are close to the conductivity reported from reference[38] (see Table S2). A comparison in conductivity among RPNPs, commercial RP, Si, and Ge pellets is shown in Figure 4b, and its corresponding *I*−*V* measurements are shown in Figure 4c. The conductivity of commercial RP was too low to be measured, whereas the conductivity observed in our synthetic RPNPs is comparable to the semiconductor. For the RPNPs, the conductivity between $2.62 \times 10^{-3}$ S m$^{-1}$ (0−0.2 V) to $1.81 \times 10^{-2}$ S m$^{-1}$ (0.7−1 V) was observed, which is $10^{10}$ orders higher than commercial RP, 100 times higher than that of intrinsic Si and slightly smaller than that of intrinsic Ge (Table S2). We speculate that the iodine doping may play a key role in the enhancement of conductivity for RPNPs. Iodine has been demonstrated as an important dopant and has been applied in conducting polymers to improve the conductivity.[39,40] In addition, iodine doping can also increase the conductivity of other materials such as carbon nanotubes[41,42] and graphene.[43,44] One of the possible reasons that the conductivity is improved by iodine doping is the enhanced density of mobile holes.[41,45,46] The drastically increased conductivity of RPNPs was expected to facility the diffusion of electrons and lithium ions, leading to ultrahigh rate capability and stable cycling performance.

The electrochemical performance of the RPNPs was tested in CR2032 coin cells using a lithium metal foil as counter electrode within the range of 0.01 to 2.5 V as the operating voltage. Figure 5a shows the cyclic voltammetry (CV) test of the RPNPs. There is a broad peak, which was ascribed to the activation process of inserting Li ions into phosphorus in the first lithiation cycle.[27,28] After the first lithiation−delithiation cycle, three peaks appeared from 1.5 to 0.01 V in the cathodic scan. The first two apparent peaks at 0.75 and 0.25 V are the continuous lithiation process to form $Li_xP$. Unlike previous reports, we consider that the most-apparent peak, from 0.25 to 0.01 V. is the final lithiation step to form $Li_3P$, which was also found in the CV test of commercial RP, as shown in Figure S4a (Supporting Information). Park and Shon also showed the ex-XRD data that only the $Li_3P$ phase exists without the other $Li_xP$ phase when the potential is near to 0 V.[19] For the anodic cycle, two peaks appeared at 1.1 and 1.25 V, which revealed the stepwise of extracting the lithium from lithium phosphide.[20,28] Figure 5b represents the voltage profiles of RPNPs cycled at a rate of 0.2 C. The RPNPs had the discharge (lithiation)−charge (delithiation) specific capacity of 2519−1861 mA h g$^{-1}$, corresponding to the Coulombic efficiency of 73.87% at the first cycle. This high irreversible capacity of 658 mA h g$^{-1}$ in the first discharge−charge step results from the decomposition of the electrolyte, which causes the formation of SEI on the electrode surface and the consumption of Li-ion.[13,25] Moreover,


DOI: 10.1021/acs.nanolett.6b05081
Nano Lett. 2017, 17, 1240−1247

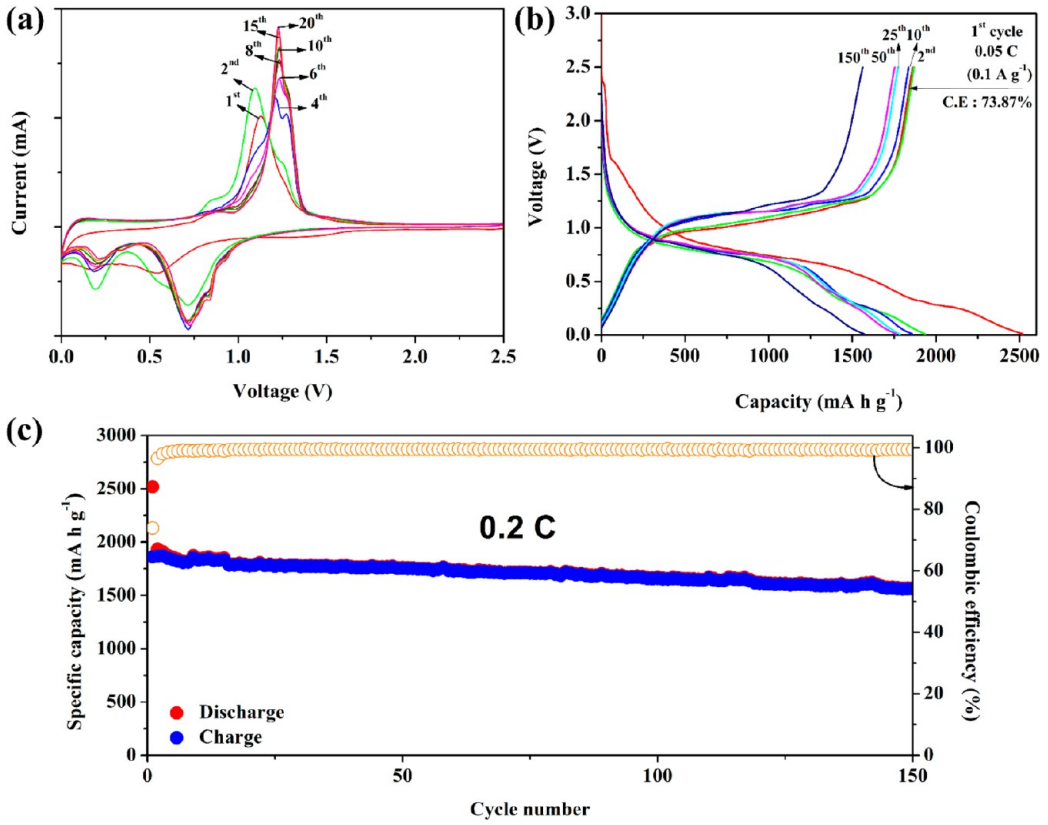


**Figure 5.** Electrochemical performance of RPNPs; 1 C = 2000 mA $g^{-1}$ (a) Cyclic voltammetry test of RPNPs at a scan rate of 0.1 mV $s^{-1}$. (b) Voltage profiles of RPNPs at a rate of 0.2 C between 0.01 and 2.5 V. (c) Cycling performance of RPNPs at a rate of 0.2 C.

nanoparticles possess a high surface area in contact with the electrolyte solution, which results in more side reactions and the formation of SEI, lowering the initial Coulombic efficiency in the first cycle.[3,9] After 150 cycles, RPNPs remained a specific charge capacity of 1562 mA h $g^{-1}$ (Figure 5c), having the retention of 83.6% with respect to the specific charge capacity of second cycle (1868 mA h $g^{-1}$).

The rate-capability of RPNPs was evaluated by changing the discharge−charge rates from 0.1 to 30 C, as shown in Figure 6a, and its corresponding voltage profiles are shown in Figure 6b. Compared to the commercial RP (Figure S4), RPNPs showed outstanding rate performance between 1 and 30 C, displaying the specific charge capacities of 1711, 1489, 1348, 1227, 984, 757, 530, 313, and 200 mA h $g^{-1}$ at the rates of 0.1, 1, 3, 5, 10, 15, 20, 25, and 30 C, respectively. Furthermore, the upper limit of the charge current density of RPNPs was investigated by varying the charge current density while the discharge rate was fixed at 0.1 C, as shown in Figure 6c. RPNPs achieved above a specific charge capacity of 1000 mA h $g^{-1}$ at the charge current density of 40 A $g^{-1}$ (20 C). Even at an ultrahigh charge current density of 120 A $g^{-1}$ (60 C), RPNPs exhibited a specific charge capacity of 175 mA h $g^{-1}$, and the plateau of RPNPs did not disappear, as shown in Figure 6d (Figure S5 shows the voltage profiles at the rates of 40, 50, and 60 C more clearly), indicating that delithiation still occurred from the RPNPs at ultrahigh charge current density. The tests of long cycling performance at different discharge/charge rates of 0.2, 1, 5, 10, and 15 C were also carried out, as shown in Figure S6. No obvious capacity fade was observed after 150 cycles for the RPNPs anode. As shown in Figure 6e, RPNPs showed good cycling life of 500 cycles at a rate of 1 C. This remarkable electrochemical performance of RPNPs could be mainly attributed to the vastly raising conductivity of the RPNPs, which is 10 000 000 000 times higher than that of bulk commercial RP (the effect of raising conductivity by iodine-doping also found in the synthetic bulk RP, which exhibited better cycling performance than commercial RP, as shown in Figure S7). Besides conductivity, RPNPs possess uniform size and smaller diameter to shorten the transport distance of electrons and lithium-ions intercalation−deintercalation[47] and endure the repetitive volume change during charge−discharge, solving the fracture issue of high-capacity materials.[3,48,49]

To demonstrate the prevention of fracture when the size of red phosphorus particles is reduced to the nanoscale, coin-type cells of RPNPs were disassembled after 100 cycles at a rate of 5 C and 500 cycles at a rate of 0.2 C (Figure S8 shows the cycling performance). Figure S9a,b are the SEM images of the pristine RPNPs electrode before lithiation, showing good dispersion of RPNPs with binders and conductive agents in electrode. After 100 cycles at the rate of 5 C, the surface of RPNPs became uneven and rough compared to original particles; however, the structure of 200 nm particles is maintained without fracture, indicating the critical fracture diameter of red phosphorus particles is at least 200 nm (Figure S9c,d). When the cycle number was extended to 500, although the surface of RPNPs became more rough, the near-spherical particles were still observed (Figure S9e,f). The TEM images in Figure S10 further confirm the change of RPNPs structure after 500 cycles, revealing that the structure of particles was intact with a rough surface. These results demonstrate that RPNPs could accommodate rapid volume expansion−contraction at high


DOI: 10.1021/acs.nanolett.6b05081
Nano Lett. 2017, 17, 1240−1247

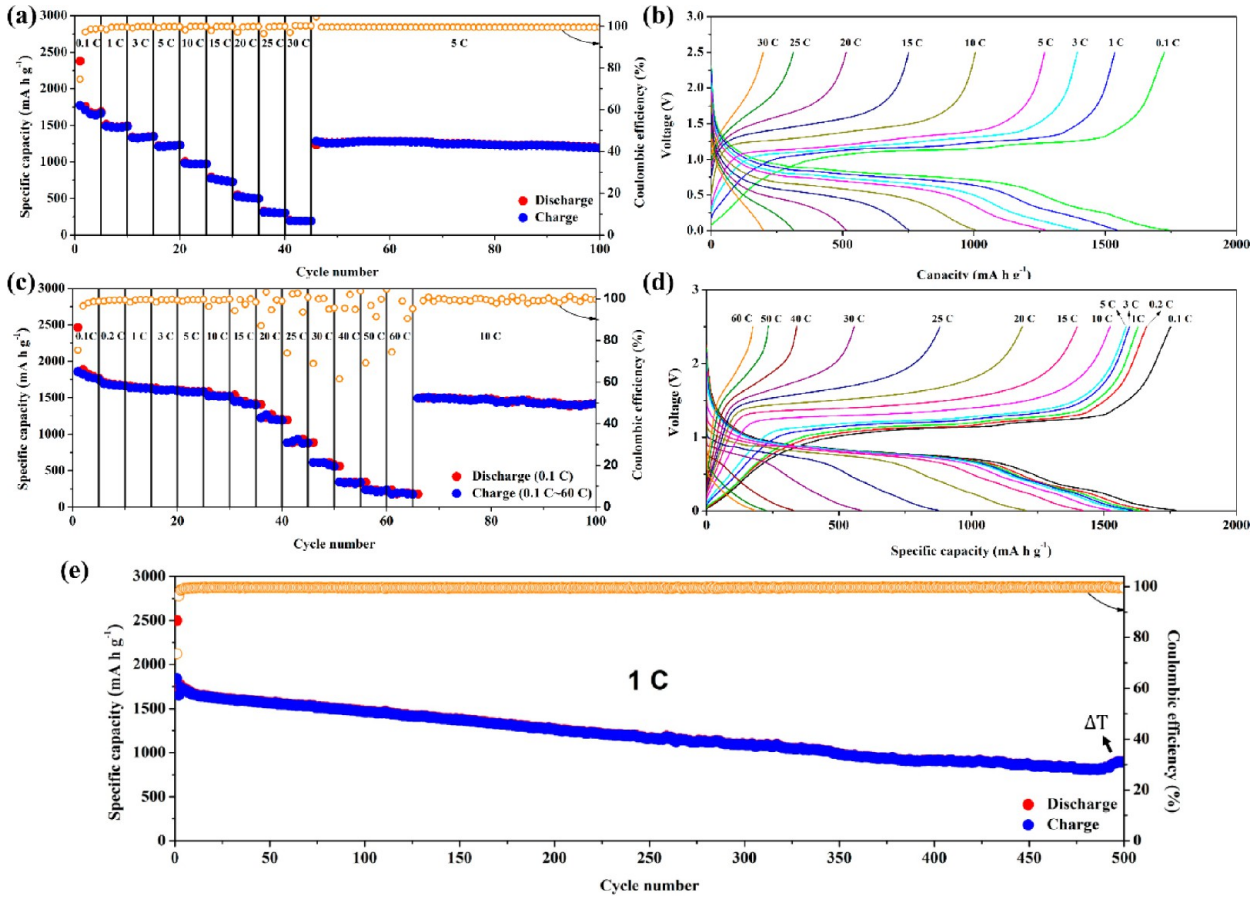


**Figure 6.** (a) The rate performance of RPNPs electrode at various rates from 0.1 to 30 C. (b) Voltage profiles of RPNPs at various rates from 0.1 to 30 C corresponding to (a). (c) The charge rate performance of RPNPs electrode at various charge rates from 0.1 to 60 C. The discharge rate was fixed at 0.1 C. (d) Voltage profiles of RPNPs at various charge rates from 0.1 to 60 C corresponding to (c). (e) The cycling performance of RPNPs at a rate of 1 C over 500 cycles. In (e), the label of $\Delta T$ was caused from the fail of air conditioner, leading the temperature to increase from 22 to 30 °C.

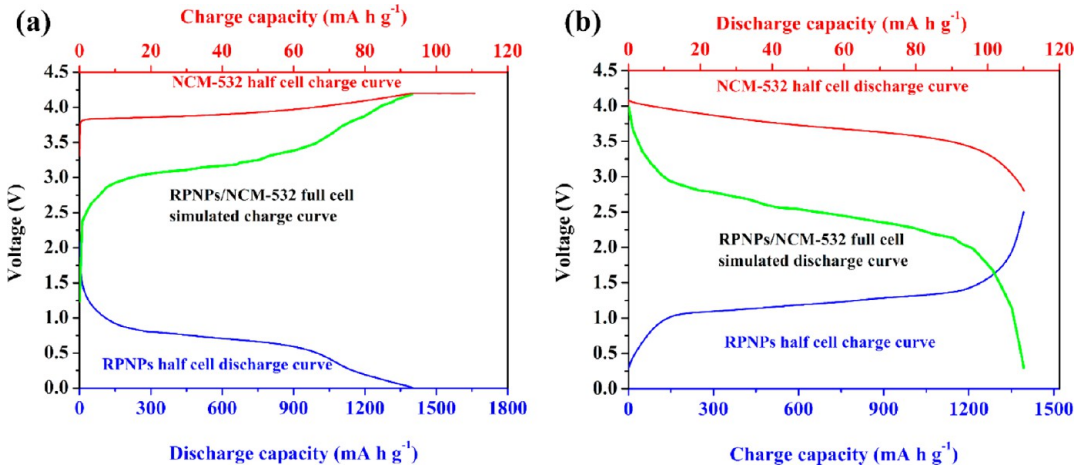


**Figure 7.** Simulation of charge−discharge curves of the RPNPs−NCM-532 full-cell at a rate of 3 C. (a) Simulation of charge curve of RPNPs−NCM-532 full cell by using NCM-532 half-cell charge curve and RPNPs half-cell discharge curve. (b) Simulation of discharge curve of RPNPs−NCM-532 full cell by using NCM-532 half-cell discharge curve and RPNPs half-cell charge curve. For NCM-532, 1 C = 160 mA $g^{-1}$. For RPNPs, 1 C = 2000 mA $g^{-1}$.

current density and repetitive volume change during long cycling process.

The first red phosphorus lithium-ion full cell comprising the RPNPs anode and the commercial $Li(Ni_{0.5}Co_{0.3}Mn_{0.2})O_2$ (NCM-532) cathode was built to demonstrate the viability of RPNPs as an LIB anode in this work. In general, setting an appropriate cutoff voltage window was required for full cells with a high capacity and the stable performance. Figure 7a shows the simulation of charge curve of RPNPs−NCM-532 full cell, which were obtained by subtracting the charge curve of the



DOI: 10.1021/acs.nanolett.6b05081
Nano Lett. 2017, 17, 1240−1247

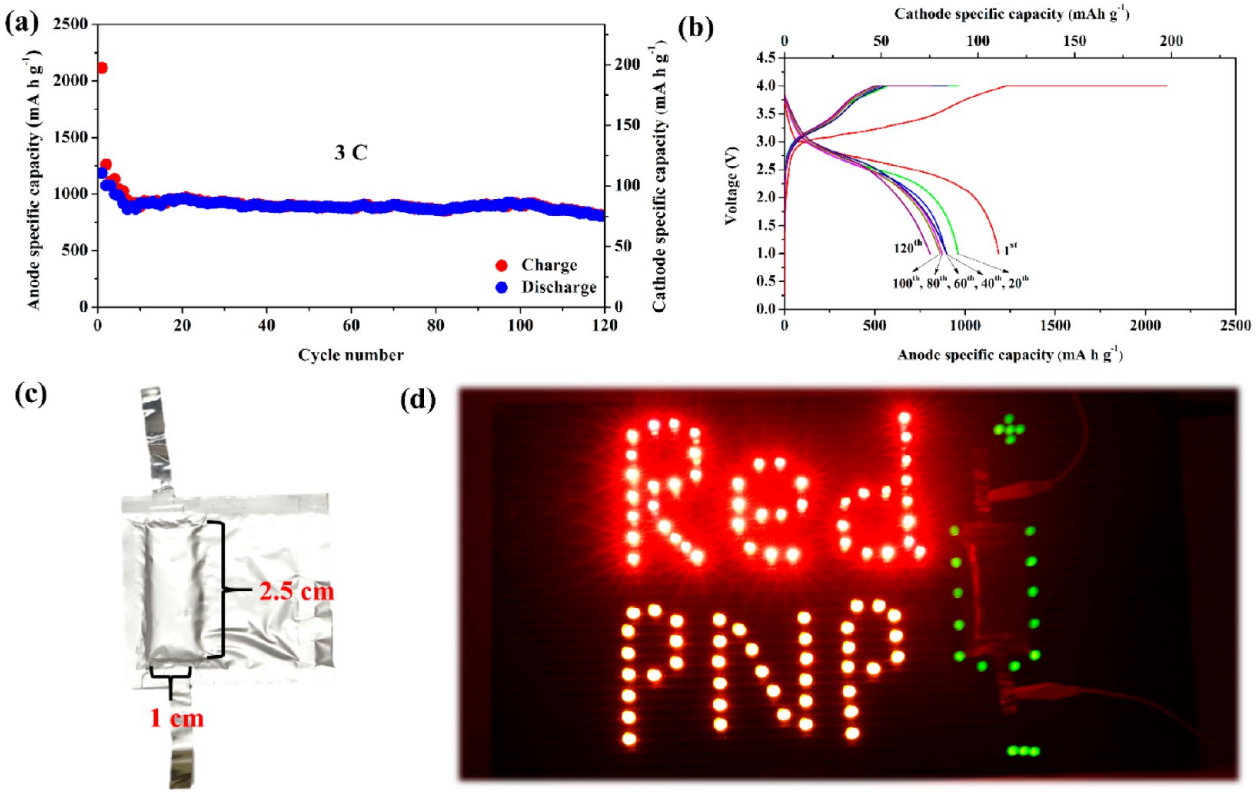


**Figure 8.** Electrochemical characteristic of the RPNPs−NCM-532 full cell and its practical application. (a) Cycling performance of coin full cell at a rate of 3 C between 1 and 4 V. (b) Voltage profiles corresponding to (a). (c) The 40 mA h pouch type battery. (d) The pouch-type battery lighted up over 100 different color LEDs.

NCM-532 from the discharge curve of the RPNPs in their respective half-cells. The charge curve of RPNPs−NCM-532 full cell should range from 2.5 to 4 V, and the charge plateau of RPNPs−NCM-532 full cell is about 3.3 V. Likewise, as shown in Figure 7b, the discharge curve of RPNPs−NCM-532 full cell was plotted in a similar way, ranging from 4 to 0.3 V. The discharge plateau of RPNPs−NCM-532 is about 2.5 V. On the basis of the simulation from half-cells, the lower and upper cutoff voltages were set to 1 and 4 V, respectively, because only few capacities of 20 mA h g$^{-1}$ could be obtained between 1 and 0.3 V.

The RPNPs−NCM-532 full cell was evaluated by using constant current-constant voltage technique (CC−CV) under the cutoff voltage window between 1 and 4 V because our cathode cannot achieve stable cycling performance at the high current density through only CC charging mode (Figure S11). As shown in Figure 8a, The RPNPs as an anode in full cell exhibited a specific charge capacity of 2117 mA h g$^{-1}$ at first cycle through the CC−CV technique, indicating high utilization of RPNPs. In the following cycles, the RPNPs−NCM-532 full cell displayed good retention of 75% (respect to the second cycle) at a rate of 3 C after 120 cycles. Figure 8b is the voltage profiles of RPNPs−NCM-532 full cell. The voltage plateau of the RPNPs−NCM-532 full cell is about 3.3 V at the charge process and 2.5 V at the discharge process, which is consistent approximately with the results of the simulation. To apply the RPNPs to practical application, a RPNPs anode and a NCM-532 cathode were wound together with a separator to form a 1 cm × 2.5 cm pouch-type battery, as shown in Figure 8c. The RPNPs battery has a capacity of 40 mA h, which can light up more than one hundred LEDs with three different colors (Figure 8d).

We show a facile solution-phase approach to synthesis iodine-doped red phosphorus nanoparticles with low energy consumption and a large scale under the ambient environment. The use of CTAB play a vital role in forming near-spherical nanoparticles with uniform size (100−200 nm), and the iodine-doping might be the key factor of improving conductivity. Therefore, RPNP is an appealing anode materials for energy storage due to the two key advantages: uniform sizes in nanoscale and high conductivity, giving favorable cyclability and outstanding high-rate capability. Compared to P−C composites, RPNPs grown from the solution-phase approach avoid a high portion of carbon in active materials and make particle size controllable. With innovative research, other chemical reactions could be designed for combining with the reaction of RPNPs to further enhance its performance in energy storage system, opening up a new promising avenue by which to design the nanostructure of red phosphorus.

## ■ ASSOCIATED CONTENT

### Supporting Information

The Supporting Information is available free of charge on the ACS Publications website at DOI: 10.1021/acs.nanolett.6b05081.

Experimental details; details on electrochemical characterization; a photograph, SEM image, and XRD and Raman spectra of RP powder obtained without adding CTAB and commercial RP powder; EDS analysis of RPNPs; images of Si, Ge, RPNPs, and RP pellets; a table summary of EDS elemental RPNPs composition; a table



DOI: 10.1021/acs.nanolett.6b05081
Nano Lett. 2017, 17, 1240−1247

summary of resistivity and conductivity values of RPNPs, Ge, Si and RP pellets; electrochemical performance of commercial RPs, synthetic bulk RP, and RPNPs; SEM and TEM images of RPNPs electrodes; and cycling performance of $Li(Ni_{0.5}Co_{0.3}Mn_{0.2})O_2$. (PDF)

## AUTHOR INFORMATION


### Corresponding Author

*E-mail: hytuan@che.nthu.edu.tw. Phone: (886)3-571-5131, extension: 42509.

### ORCID

Hsing-Yu Tuan: 0000-0003-2819-2270


### Notes

The authors declare no competing financial interest.

## ACKNOWLEDGMENTS

We acknowledge the financial support by the Ministry of Science and Technology through grant nos. NSC 102-2221-E-007-023-MY3, MOST 103-2221-E-007-089-MY3, MOST 103-2622-E-007-025, and MOST 102−2633-M-007-002.

## REFERENCES


(1) Janek, J.; Zeier, W. G. *Nat. Energy* **2016**, *1*, 16141.
(2) Szczech, J. R.; Jin, S. *Energy Environ. Sci.* **2011**, *4*, 56−72.
(3) Sun, Y.; Liu, N.; Cui, Y. *Nat. Energy* **2016**, *1*, 16071.
(4) Bogart, T. D.; Chockla, A. M.; Korgel, B. A. *Curr. Opin. Chem. Eng.* **2013**, *2*, 286−293.
(5) Wu, S.; Han, C.; Iocozzia, J.; Lu, M.; Ge, R.; Xu, R.; Lin, Z. *Angew. Chem., Int. Ed.* **2016**, *55*, 7898−7922.
(6) Wu, H.; Chan, G.; Choi, J. W.; Ryu, I.; Yao, Y.; McDowell, M. T.; Lee, S. W.; Jackson, A.; Yang, Y.; Hu, L.; Cui, Y. *Nat. Nanotechnol.* **2012**, *7*, 310−315.
(7) Kennedy, T.; Mullane, E.; Geaney, H.; Osiak, M.; O'Dwyer, C.; Ryan, K. M. *Nano Lett.* **2014**, *14*, 716−723.
(8) Bogart, T. D.; Oka, D.; Lu, X.; Gu, M.; Wang, C.; Korgel, B. A. *ACS Nano* **2014**, *8*, 915−922.
(9) Liu, N.; Lu, Z.; Zhao, J.; McDowell, M. T.; Lee, H.-W.; Zhao, W.; Cui, Y. *Nat. Nanotechnol.* **2014**, *9*, 187−192.
(10) Liu, N.; Wu, H.; McDowell, M. T.; Yao, Y.; Wang, C.; Cui, Y. *Nano Lett.* **2012**, *12*, 3315−3321.
(11) Ngo, D. T.; Le, H. T. T.; Kim, C.; Lee, J.-Y.; Fisher, J. G.; Kim, I.-D.; Park, C.-J. *Energy Environ. Sci.* **2015**, *8*, 3577−3588.
(12) Kang, D.-Y.; Kim, C.; Gueon, D.; Park, G.; Kim, J. S.; Lee, J. K.; Moon, J. H. *ChemSusChem* **2015**, *8*, 3414−3418.
(13) Yuan, F.-W.; Tuan, H.-Y. *Chem. Mater.* **2014**, *26*, 2172−2179.
(14) Hembram, K. P. S. S.; Jung, H.; Yeo, B. C.; Pai, S. J.; Kim, S.; Lee, K.-R.; Han, S. S. *J. Phys. Chem. C* **2015**, *119*, 15041−15046.
(15) Sun, J.; Zheng, G.; Lee, H.-W.; Liu, N.; Wang, H.; Yao, H.; Yang, W.; Cui, Y. *Nano Lett.* **2014**, *14*, 4573−4580.
(16) Extance, P.; Elliott, S. R. *Philos. Mag. B* **1981**, *43*, 469−483.
(17) Bai, A.; Wang, L.; Li, J.; He, X.; Wang, J.; Wang, J. *J. Power Sources* **2015**, *289*, 100−104.
(18) Li, W.-J.; Chou, S.-L.; Wang, J.-Z.; Liu, H.-K.; Dou, S.-X. *J. Mater. Chem. A* **2016**, *4*, 505−511.
(19) Park, C. M.; Sohn, H. J. *Adv. Mater.* **2007**, *19*, 2465−2468.
(20) Qian, J.; Qiao, D.; Ai, X.; Cao, Y.; Yang, H. *Chem. Commun.* **2012**, *48*, 8931−8933.
(21) Ramireddy, T.; Xing, T.; Rahman, M. M.; Chen, Y.; Dutercq, Q.; Gunzelmann, D.; Glushenkov, A. M. *J. Mater. Chem. A* **2015**, *3*, 5572−5584.
(22) Kim, Y.; Park, Y.; Choi, A.; Choi, N.-S.; Kim, J.; Lee, J.; Ryu, J. H.; Oh, S. M.; Lee, K. T. *Adv. Mater.* **2013**, *25*, 3045−3049.
(23) Qian, J.; Wu, X.; Cao, Y.; Ai, X.; Yang, H. *Angew. Chem., Int. Ed.* **2013**, *52*, 4633−4636.
(24) Wang, L.; He, X.; Li, J.; Sun, W.; Gao, J.; Guo, J.; Jiang, C. *Angew. Chem., Int. Ed.* **2012**, *51*, 9034−9037.
(25) Li, W.; Yang, Z.; Li, M.; Jiang, Y.; Wei, X.; Zhong, X.; Gu, L.; Yu, Y. *Nano Lett.* **2016**, *16*, 1546−1553.
(26) Li, W.-J.; Chou, S.-L.; Wang, J.-Z.; Liu, H.-K.; Dou, S.-X. *Nano Lett.* **2013**, *13*, 5480−5484.
(27) Yuan, D.; Cheng, J.; Qu, G.; Li, X.; Ni, W.; Wang, B.; Liu, H. *J. Power Sources* **2016**, *301*, 131−137.
(28) Yu, Z.; Song, J.; Gordin, M. L.; Yi, R.; Tang, D.; Wang, D. *Adv. Sci.* **2015**, *2*, 1400020.
(29) Zhang, C.; Wang, X.; Liang, Q.; Liu, X.; Weng, Q.; Liu, J.; Yang, Y.; Dai, Z.; Ding, K.; Bando, Y.; Tang, J.; Golberg, D. *Nano Lett.* **2016**, *16*, 2054−2060.
(30) Song, J.; Yu, Z.; Gordin, M. L.; Hu, S.; Yi, R.; Tang, D.; Walter, T.; Regula, M.; Choi, D.; Li, X.; Manivannan, A.; Wang, D. *Nano Lett.* **2014**, *14*, 6329−6335.
(31) Sun, J.; Lee, H.-W.; Pasta, M.; Yuan, H.; Zheng, G.; Sun, Y.; Li, Y.; Cui, Y. *Nat. Nanotechnol.* **2015**, *10*, 980−985.
(32) Sun, J.; Lee, H.-W.; Pasta, M.; Sun, Y.; Liu, W.; Li, Y.; Lee, H. R.; Liu, N.; Cui, Y. *Energy Storage Materials* **2016**, *4*, 130−136.
(33) Gao, H.; Zhou, T.; Zheng, Y.; Liu, Y.; Chen, J.; Liu, H.; Guo, Z. *Adv. Energy Mater.* **2016**, *6*, 1601037.
(34) Zhang, Y.; Rui, X.; Tang, Y.; Liu, Y.; Wei, J.; Chen, S.; Leow, W. R.; Li, W.; Liu, Y.; Deng, J.; Ma, B.; Yan, Q.; Chen, X. *Adv. Energy Mater.* **2016**, *6*, 1502409.
(35) Qi, W. H.; Wang, M. P. *Mater. Chem. Phys.* **2004**, *88*, 280−284.
(36) Zeng, X.-R.; Ko, T.-M. *J. Polym. Sci., Part B: Polym. Phys.* **1997**, *35*, 1993−2001.
(37) Yao, Z.; Nie, H.; Yang, Z.; Zhou, X.; Liu, Z.; Huang, S. *Chem. Commun.* **2012**, *48*, 1027−1029.
(38) Serway, R. A.; Jewett, J. W. *Physics for Scientists and Engineers with Modern Physics*, 9th ed.; Cengage Learning, 2013.
(39) Jiang, Z.; Sen, A. *Macromolecules* **1992**, *25*, 880−882.
(40) Yang, T.; Wang, H.; Ou, X.-M.; Lee, C.-S.; Zhang, X.-H. *Adv. Mater.* **2012**, *24*, 6199−6203.
(41) Zhao, Y.; Wei, J.; Vajtai, R.; Ajayan, P. M.; Barrera, E. V. *Sci. Rep.* **2011**, *1*, 83.
(42) Behabtu, N.; Young, C. C.; Tsentalovich, D. E.; Kleinerman, O.; Wang, X.; Ma, A. W. K.; Bengio, E. A.; ter Waarbeek, R. F.; de Jong, J. J.; Hoogerwerf, R. E.; Fairchild, S. B.; Ferguson, J. B.; Maruyama, B.; Kono, J.; Talmon, Y.; Cohen, Y.; Otto, M. J.; Pasquali, M. *Science* **2013**, *339*, 182−186.
(43) Zhan, Y.; Zhang, B.; Cao, L.; Wu, X.; Lin, Z.; Yu, X.; Zhang, X.; Zeng, D.; Xie, F.; Zhang, W.; Chen, J.; Meng, H. *Carbon* **2015**, *94*, 1−8.
(44) Pei, S.; Zhao, J.; Du, J.; Ren, W.; Cheng, H.-M. *Carbon* **2010**, *48*, 4466−4474.
(45) Jaiswal, M.; Menon, R. *Polym. Int.* **2006**, *55*, 1371−1384.
(46) Lee, R. S.; Kim, H. J.; Fischer, J. E.; Thess, A.; Smalley, R. E. *Nature* **1997**, *388*, 255−257.
(47) Arico, A. S.; Bruce, P.; Scrosati, B.; Tarascon, J.-M.; van Schalkwijk, W. *Nat. Mater.* **2005**, *4*, 366−377.
(48) Liang, W.; Yang, H.; Fan, F.; Liu, Y.; Liu, X. H.; Huang, J. Y.; Zhu, T.; Zhang, S. *ACS Nano* **2013**, *7*, 3427−3433.
(49) Liu, X. H.; Zhong, L.; Huang, S.; Mao, S. X.; Zhu, T.; Huang, J. Y. *ACS Nano* **2012**, *6*, 1522−1531.




DOI: 10.1021/acs.nanolett.6b05081
*Nano Lett.* 2017, 17, 1240−1247